Breaking through permeability-selectivity trade-off of thin-film composite membranes assisted with crown ethers

Liang Shen [a,b], Ming Yi [a,b], Susilo Japip [c], Lian Tian [a,b], Cher Hon Lau [d]* and Yan Wang [a,b]*

[a] Key Laboratory of Material Chemistry for Energy Conversion and Storage (Huazhong University of Science and Technology), Ministry of Education, Wuhan, 430074, P.R. China

[b] Hubei Key Laboratory of Material Chemistry and Service Failure, School of Chemistry and Chemical Engineering, Huazhong University of Science & Technology, Wuhan, 430074, P. R. China

[c] Department of Chemical and Biomolecular Engineering, National University of Singapore, Singapore 117576, Singapore

[d] School of Engineering, The University of Edinburgh, Robert Stevenson Road, Edinburgh EH9 3FB, United Kingdom

* Corresponding authors. Tel.: 86 027 87543032; fax: 86 027-87543632.

E-mail address: wangyan@hust.edu.cn (Yan Wang)

Tel.: +44 131 650 7813 .

E-mail address: Cherhon.Lau@ed.ac.uk (Cher Hon Lau)

Abstract

In this study, we deployed a modified interfacial polymerization process to incorporate multifunctional crown ethers (CEs) into thin-film composite (TFC) polyamide membranes. These CE additives acted as both the phase-transfer catalyst and co-solvent to facilitate the diffusion of amine monomers into the organic phase and also enhanced the free volume content of the selective layer, facilitating water transport and inhibiting the diffusion of draw solutes. Various characterization techniques were employed to elucidate the modification mechanism as a function of CE chemical and physical properties on the microstructure of resultant TFC membranes and consequently separation performances. Compared to TFC membranes produced from traditional interfacial polymerization method, CE-modified membranes exhibited a 146% water flux enhancement and 59% lower reverse salt fluxes with a suitable draw solution. CE-modified membranes also exhibited improved antifouling performance with a lower flux drop (34% decline) and a higher flux recovery ratio (38% improvement).

Keywords: Thin-Film Composite Membrane; Polyamide; Crown Ether; Interfacial Polymerization; Permeability-Selectivity Trade-off

1. INTRODUCTION

By 2050, the global population will increase by 2 billion, reaching 9.7 billion people.[1] Key to sustaining this burgeoning growth is overcoming water scarcity for anthropogenic activities.[2] Various water treatment technologies have been exploited in the past few decades to produce clean water.[3-6] For example, membrane-based separation techniques such as ultrafiltration,[7,8] nanofiltration,[9-11] reverse osmosis[12,13] and forward osmosis (FO)[14-16] have been implemented at various levels for desalination, wastewater and water treatment. The heart of the successful implementation of these technologies is a high-performance membrane with superior separation efficiency and excellent fouling resistance. Since the commercialization of thin-film composite (TFC) membranes in the 1970s,[17] such membranes are preferred in the industry for their high fluxes, reasonable selectivity and ease of fabrication. TFC membranes are generally produced by interfacial polymerization (IP) of aromatic amine monomers dissolved in an aqueous solution and an organic solution containing acyl chloride monomers to form a dense aromatic polyamide (PA) layer on a porous support layer.[18-21] Both the reaction rate and degree of the polymerization are determined by the solubility of the reactive monomer in the opposite phases i.e. the diffusion rate of amine monomers from the aqueous phase into the organic phase.[22] Hence the diffusion-limited growth of PA chains coupled with the extremely fast polymerization kinetics between both highly reactive monomers typically result in poor control over bulk properties and microstructure of the formed PA layer, consequently impacting on the separation performances of resulting TFC membranes.

The IP process can be tailored *via* various approaches to enhance separation properties from an optimized PA microstructure. For example, the addition of catalytic

additives[23] in the monomer solution or a co-solvent system[22] altered diffusion rates of amine monomers into the organic phase and IP kinetics that consequently optimized bulk properties and enhanced separation performances. Alternatively, effervescence i.e. formation of nanosized gas bubbles in the amine solution *via* ultrasonication or addition of $NaHCO_3$ to the amine solution also impacted on the morphology and separation performances of TFC membranes.[24] Similarly, we recently showed that ultrasonication during IP was effective for facilitating efficient mixing of two monomer phases that optimized free volume size and content in the PA layer.[25,26] Additionally, the thickness, roughness and chemical composition of the PA layer could be controlled by molecular layer-by-layer deposition method reported recently, to yield maximum separation performances, where molecular transport was not impeded by kinetic and mass transfer limitations associated with the traditional IP process.[27] It also can be achieved by employing an intermediate layer of nanostrands that regulated the release of amine monomers at the water-hexane interface, providing precise control over the PA morphology and thickness.[28] Besides, 3D printed PA membranes developed by electrospraying of monomers on to a substrate also provided precise control over film thickness and roughness.[29] Recently, Wang *et. al.* reported a nanostructure-mediated IP process to prepare rough PA layers with extensively crumpled nanoscale structures.[30] The combination of these unique nanoscale membrane topologies led to unprecedented permeances, which were realized by preloading sacrificial templating nanoparticles on a substrate.[30]

Different from these studies, here we incorporated crown ethers (CE) in the monomer solution to tailor the formation of aggregate and network pores within PA selective layers of TFC membranes that were crucial for addressing the tradeoff relationship between permeability and selectivity (**Figure 1**). These membranes were

applied in FO for the first time. CE, a cyclic polyether, is miscible with both water and organic solvents[31] and is an excellent chelating agent with intrinsic cavities that are selective towards metal ions (especially for alkali metal ions).[32] Therefore, it is widely used as the phase-transfer catalyst in organic reactions to transfer inorganic reaction reagents into the organic phase, accelerating chemical reactions.[32] Moreover, the inner and outer of the CE cavity are hydrophilic and lipophilic, respectively. Ascribing to these unique characteristics of CE, we hypothesized that CE-assisted IP could significantly impact on the microstructure, morphology as well as FO performances of resulting TFC membranes. This hypothesis was underpinned by two main attributes. First, the miscibility of CE with organic solvents such as hexane and the ability to form hydrogen bonds with amine monomers enable CE to act as a co-solvent and phase-transfer catalyst to enhance amine diffusion into the organic phase, contributing to a more complete IP reaction. Second, the hydrophilicity of CEs could be harnessed to improve the water permeance of resultant PA films during FO whilst chelating metal ions of draw solutes (NaCl and KCl used in this study), contributing to less draw solute leakage. We systemically verified these hypotheses using a series of complementary characterization techniques to elucidate the effects of various modification routes (adding in the aqueous or organic phase), CE type and concentration, as well as the draw solute type are investigated systematically in this study.

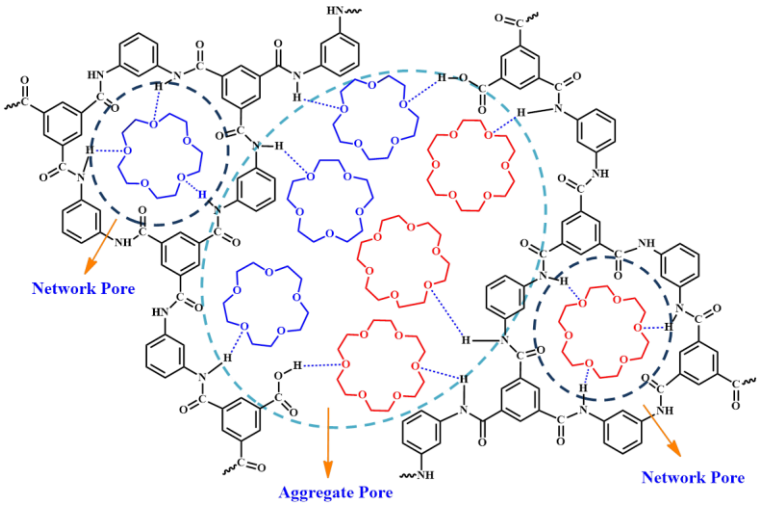

FIGURE 1 Schematic illustration of PA networks with CE15 and CE18 incorporated

2. EXPERIMANTAL

2.1 Materials

M-phenylenediamine (MPD, 99.5%) and 1, 3, 5-benzenetricarbonyl trichloride (TMC, 98%) were bought from Aladdin and kept in a refrigerator before use. Polysulfone (PSf) (Mw = 800,000 Da) was obtained from Beijing HWRK Chem co. Ltd. (China). PSf was dried overnight in a vacuum oven at 80 °C prior use. Polyethylene glycol 400 (PEG 400, CP), N-methyl pyrrolidone (NMP, anhydrous, ≥99.5%), n-hexane (≥97%, anhydrous), 18-crown-6 (CE18, 99%, powder), 15-crown-5 (CE15, 99%, liquid), sodium alginate (SA, Mw: 98.11), potassium dihydrogen phosphate (KH_2PO_4, 99.5%), magnesium sulfate ($MgSO_4$, 99%), sodium sulfate (Na_2SO_4, 99%), sodium bicarbonate ($NaHCO_3$, 99.5%), ammonium chloride (NH_4Cl, 99.5%), calcium chloride ($CaCl_2$, 96%) and sodium chloride (NaCl, ≥99.5%) were purchased from China National Medicine Corporation.

2.2 Preparation of TFC membranes

The PSf substrate membrane was fabricated using the non-solvent induced phase separation method.[33,34] Briefly, a degassed dope solution (PSf/PEG-400/NMP: 18/16/66 wt.%) was poured onto a clean glass plate and cast with a casting knife (3520-8, Elcometer, UK) to obtain at thickness of 100 μm. The PSf substrate was immediately immersed into a coagulation bath at room temperature to start the phase inversion process. To remove trapped solvent molecules in the PSf substrate, the water was changed every 12 hours for 2 days. These substrates were stored in deionized (DI) water that was changed every 12 h to remove residual NMP.

CE-modified TFC membranes were fabricated by adding CE into the aqueous (1 – 9 wt.% of CE15 or 3 wt.% of CE18) or organic phase (3 wt.% of CE15 or CE18) prior IP. Detailed compositions of the two monomer solutions studied here are listed in **Table S1**. Depending on the type of CE used, 18-crown-6 or 15-crown-5, CE-modified membranes were denoted as CE(A/O)-18/15-X where "A" and "O" represents the deployment of CE in the aqueous or organic phase, respectively, and "X" stands for the CE content. The miscibility of CE15 and solubility of CE18 in water and hexane (**Figure S1** and **Table S2**) were exploited here to underpin in-situ modification of PA selective layers of as-fabricated TFC membranes. The intrinsic cavities of CE18 molecules ranged from 2.6 – 3.3 Å in diameter (**Figure 2**),[32,35-37] which are ideal for permeating water molecules (dynamic diameter of 2.6 Å).[22] Meanwhile, the cavity diameters of CE15 molecules are significantly smaller (1.7-2.2 Å) and are impermeable for water molecules.[32,35-37] These differences in cavity diameters also favor stable chelation of various cations where CE15 and CE18 molecules preferentially chelate Na^+ (1.90 Å) and K^+ (2.66 Å) ions, respectively.

[19,37,38] Pristine PSf membranes were immersed in an aqueous MPD/crown ether (3.4/0 – 9 wt.%) mixture for 2 min firstly. Excess MPD solution was removed carefully from the substrate surface using a rubber roller. Next, the TMC/crown ether/hexane solution (0.15/0 – 3/100 w/w/v) was poured on to the membrane top surface and left for 1 min before draining off. The newly formed TFC membranes were washed with DI water and stored in DI water before use.

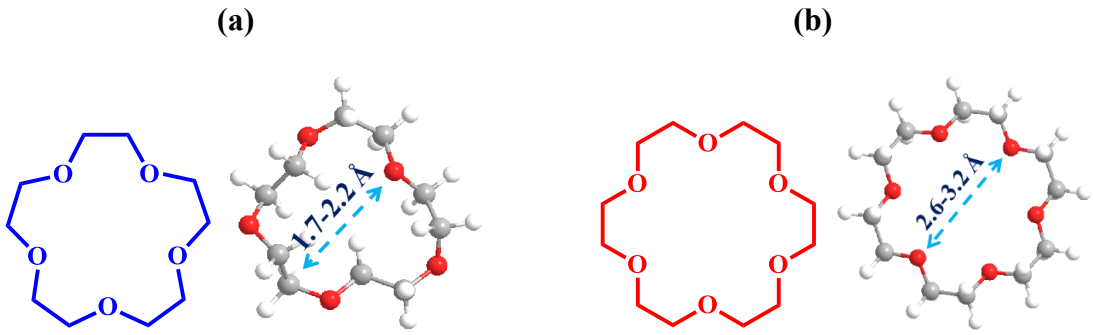

FIGURE 2 Molecular structures and intrinsic cavity diameter of (a) CE15 and (b) CE18

2.3 Characterizations of TFC membranes

Changes in the chemical structures of TFC membranes were characterized using Fourier Transform Infrared spectroscopy in the Attenuated Total Reflectance mode (ATR-FTIR, Brucker, VERTEX-70) and X-ray Photoelectron Spectroscopy (XPS, VG Multilab 2000, Thermo VG Scientific, UK) where a monochromatic A1 Ka X-ray source was employed. The free volume content of the PA layer micro-structure was characterized using Positron Annihilation Spectroscopy (PAS, National University of Singapore) *via* a variable mono-energy slow positron beam.[39] The inter-chain distance (*d*-spacing) of the PA layer was examined using X-ray diffractometer (XRD,

SmartLab-SE, Rigaku, Japan) with 2θ ranging from 10° to 60°. Surface hydrophilicity of TFC membranes was evaluated using the water contact angle (WCA) measured by a Contact Angle Goniometer (DSA 25, KRÜSS, Germany). Zeta potentials of TFC membrane were measured at 25 °C by a Zeta Potential Analyzer (SurPASS™ 3, Anton Paar, Austria) using 0.001M KCl aqueous solution with pH of 2–10. The surface morphology and topology of TFC membranes were observed by a Scanning Electron Microscope (SEM, VEGA3, TESCAN, Czech) and Atomic Force Microscope (AFM, SPM9700, Shimadzu, Japan) respectively.

2.4 Evaluation of separation performance

A lab-scale FO apparatus was employed to perform FO tests around 22±0.5 °C, using DI water and 2.0 M NaCl aqueous solution as the feed and draw solutions, respectively. All membrane samples were tested for at least three times under both FO mode (active layer facing feed solution, AL-FS orientation) and PRO mode (active layer facing draw solution, AL-DS orientation). Each test was stabilized for 30 minutes before data collection. Weight changes in the draw solution side were detected by a digital weight balance (FX3000-GD, AND, Japan). Additionally, concentration changes in the feed solution were monitored using a conductivity meter (FE30, Mettler Toledo, Switzerland). Water flux (*Jv*) and reverse salt flux (*Js*) were determined to evaluate FO performance of TFC membranes, as defined by ***Eq*s. (1)** and **(2)**.

$$J_v = \frac{\Delta V}{A_m \Delta t} \quad (1)$$

$$J_s = \frac{\Delta (C_t V_t)}{A_m \Delta t} \quad (2)$$

where ΔV is the volume change in the draw solution side over a predetermined time

(Δt), A_m is the effective membrane area in FO test (3.87 cm^2), C_t and V_t are the salt concentration and volume of the feed solution, respectively.

2.5 Dynamic fouling tests

Following well-established protocols described in our previous works, [36, 37] we performed dynamic fouling tests in the FO mode at 22±0.5 °C using synthetic wastewater and 2.0 M NaCl aqueous solution as the feed and draw solutions, respectively. Fresh membrane samples were stabilized by using DI water as both feed and draw solutions for 30 min. The initial FO flux was measured after reaching steady state by replacing DI water with 2 M NaCl solution as the draw solution. Next, the fouling process was conducted by replacing DI water in the feed solution with synthetic wastewater for 18 h (The fouling process time is 18 h using synthetic wastewater as the feed solution). The flow rate in above stages were maintained at 0.3 L/min. Fouled membranes were flushed with DI water as both feed and draw solutions at a flow rate of 0.6 L/min for 30 min. Finally, the FO fluxes of cleaned membrane were measured again.

2.6 Evaluation of CE stability in modified PA layers

CE stability in the modified PA layer was evaluated by a long-term FO test and vigorous agitation. For the long-term (72 h) FO test, a large amount of draw solution (4 L 2 M NaCl or KCl solution) and feed solution (4 L DI water) were employed to mitigate dilution effects of draw solutions and the concentration effects of feed solutions. The vigorous agitation treatment was conducted by immersing fresh

membrane samples (25 cm^2) into a centrifuge tube with 50 mL ultrapure water, which was fixed in an oscillator for 7 days, with daily water changes. The amount of CE released in the ultrapure water after various treatment durations were characterized using a Total Organic Carbon analyzer (TOC, Vario, Elementar, Germany).

3. RESULTS AND DISCUSSION

3.1 Modification mechanism

The impact of CEs on the physicochemical structure of PA was characterized by FTIR analyses and validated by XPS (**Figure 3**). From the FTIR spectra of membranes studied here (**Figure 3a**), we observed peaks centered at 1624 and 1548 cm^{-1} that were characteristic to CO-NH groups i.e. amide bonds.[40] The presence of CE in modified PA selective layers was validated by additional peaks centered at 1085 and 986 cm^{-1} that are correlated to the ether functional group[41,42] that are unique to CE across all membranes studied in this work. Interestingly, the intensity of the peak centered at 3460 cm^{-1} (stretching vibration of -OH) was reduced in CE-modified membranes. We hypothesize that the more complete IP reactions were facilitated by CE-assisted amine diffusion/dissolution in the organic phase that resulted in efficient mixing of both reactive monomers. This contradicts the principles of IP where amine molecules are typically insoluble in organic phases.[18,22] This hypothesis was validated from FTIR analyses where hydrogen bonding between amine molecules and hexane in the presence of CE were observed (**Figure S2**).

Quantitative evidence of CE presence in PA selective layers was observed from XPS analyses (**Figure 3b**). OII (*O-C/H-*O-C/C-*O-C, BE=532.2 eV)[43] and CII

(*C-OR, BE=285.4 eV)[44] peaks that corresponded to ether functional groups were only present in CE-modified PA membranes where both the OII% and CII% (peak area ratio) of the CE15-modified membrane were larger than those modified by CE18 molecules (**Figure S3**). Based on our hypothesis, as more CE molecules are present, the IP reaction would be more complete. This was also observed from the larger increase in O/N ratio (**Table S3** and **Figure S4**) where N is unique to PA and the increase in O content was primarily due to CE and higher intensity ratio of $I_{OIII/OI}$ (OIII corresponded to O atoms in carboxylic acid groups hydrolyzed from residual TMC acyl chloride groups and OI was correlated to unreacted TMC carbonyl). Both O/N and $I_{OIII/OI}$ ratios of CE15-modified membranes were higher than those of CE18-modified membranes. Attributing to a smaller molecular weight that facilitated better diffusion of CE15 into hexane, the O/N ratio in PA membranes modified by CE15 molecules was larger than that of membranes modified by CE18. TGA results also revealed that weight losses of CE-modified PA powders in the second stage (200-800 ℃, caused by the thermochemical decomposition of PA chains) were lower than those of pristine PA powders, possibly due to the intermolecular hydrogen bond interaction between PA chains and embedded CEs, indicating the stable incorporation of CEs in the PA network (**Figure S5).**

The deployment of CE as co-solvent or phase-transfer catalysts during IP also led to the formation of rougher PA layers as confirmed by SEM and AFM images in **Figures 3c-d**. **Figure 3c** also revealed that pristine PA membranes were thinner with more nodular-like surfaces, while thicker CE-modified membranes comprised obvious leaf-like and flake-like structures. Accordingly, as shown in **Figure 3d**, the surfaces of CE-modified membranes were rougher than pristine membranes, and the average roughness (*Ra*) increased with higher CE concentration or smaller CE

molecular weight (**Figure 3e**). However, the WCAs of CE-modified membranes were lower than those of pristine membranes, contradicting the *Ra* trends (**Figure 3e**). This was ascribed to the intrinsic hydrophilicity of CEs and rougher surface of CE-modified PA layers. Additionally, the lower carboxyl content in CE-modified PA i.e. higher IP conversion rates also attributed to higher zeta potential values at the same pH condition and the corresponding higher isoelectric points in CE-modified membranes (**Figure 3f**).

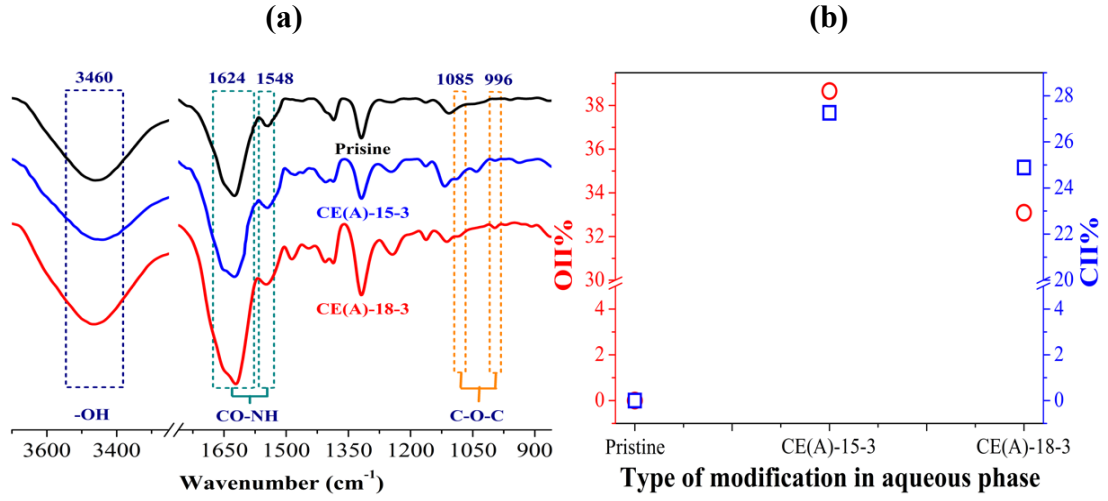

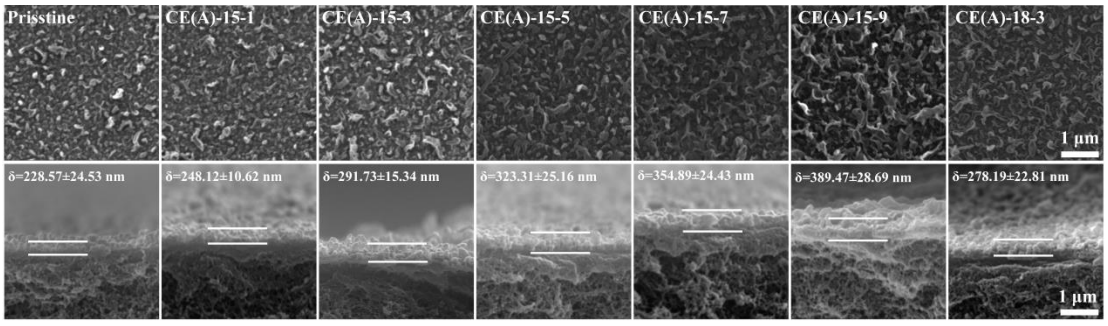

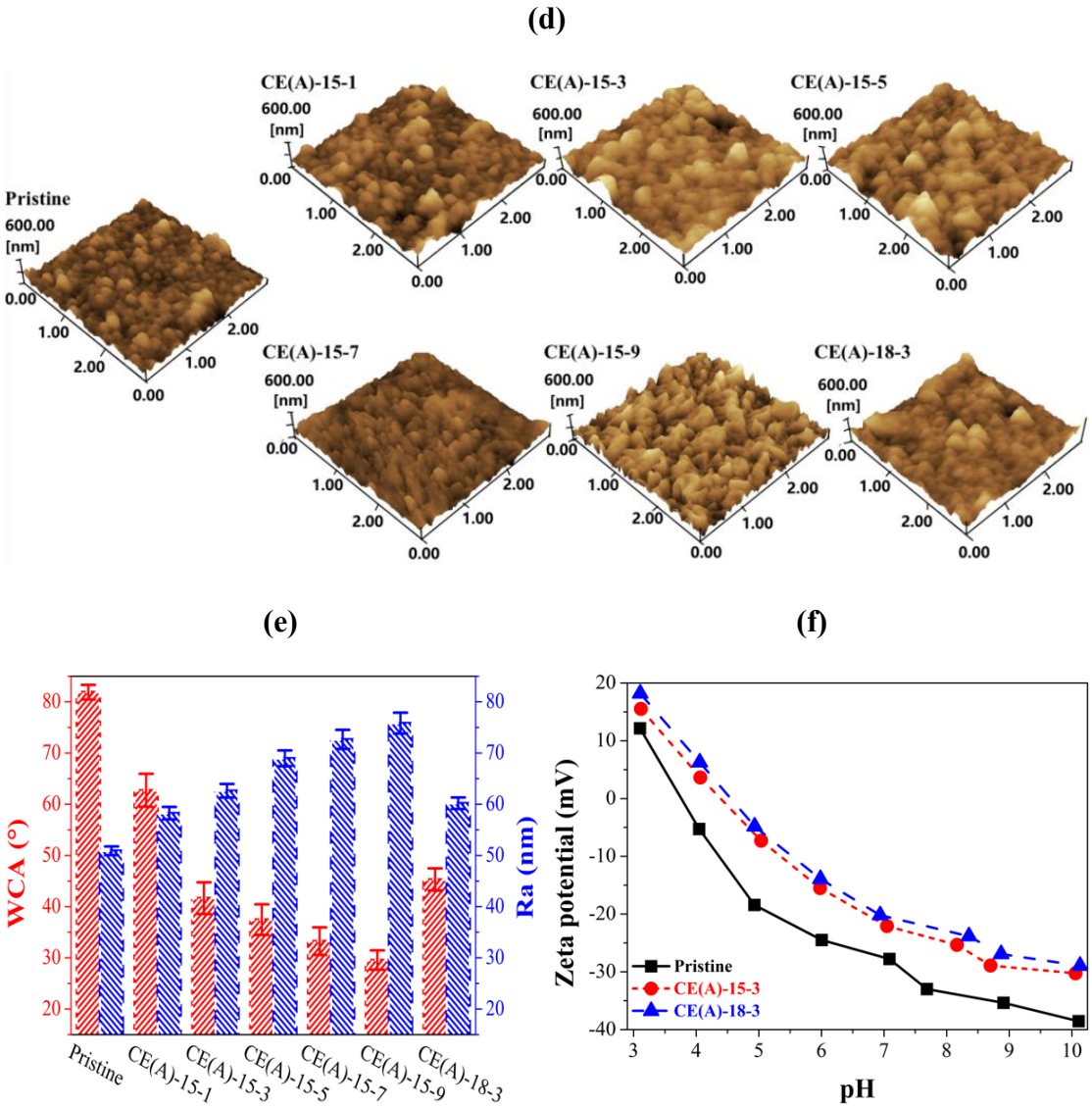

FIGURE 3 (a) FTIR spectra, **(b)** OII and CII peak area ratios, **(c)** SEM, **(d)** AFM, **(e)** water contact angles (WCA) and average roughness (*Ra*), **(f)** zeta potentials of the pristine and CE-modified membranes

Structural changes induced by CE in the resulting PA layers were characterized by PAS and XRD (**Figure 4**). PAS results based on Doppler Broadening Energy Spectrum providing qualitative information about free volume, can be reflected by *S* parameter, which is defined as the ratio of total annihilation counts at central region (511 keV).[45,46] Generally, *S* measures free volumes between 0.1 and 1 nm based on 2γ

annihilation. Higher *S* values typically indicate the more and/or larger free volume cavities in the polymer matrix, resulting in a looser structure.[45] In this study, *S* value at around 2 keV indicating the top PA layer was applied to estimate the free volume. *S* values in CE-modified membranes were larger than those of the pristine membranes (**Figures 4a** and **S6**), indicating the formation of looser PA layers with larger free volume content. The *S* value also increased as a function of CE15 content, CE molecular weight and intrinsic cavity size. Clearly, the effects of 9 wt.% of CE15 on microstructure and porosity could be achieved with 3 wt.% of CE18. The increases in free volume content and size were due to the enlargement of inter-PA chain distances caused by the addition of CE, where additives typically affect chain packing density.[22,47] The interchain distance increased from 4.834 Å to 5.014 Å as CE15 concentration increased from 1 to 9 wt.% (**Figures 4b** and **S7**). Meanwhile, the incorporation of 3 wt.% of CE18 could achieve the same effect as 9 wt.% of CE15, propping PA chains apart by 5.001 Å.

(a)

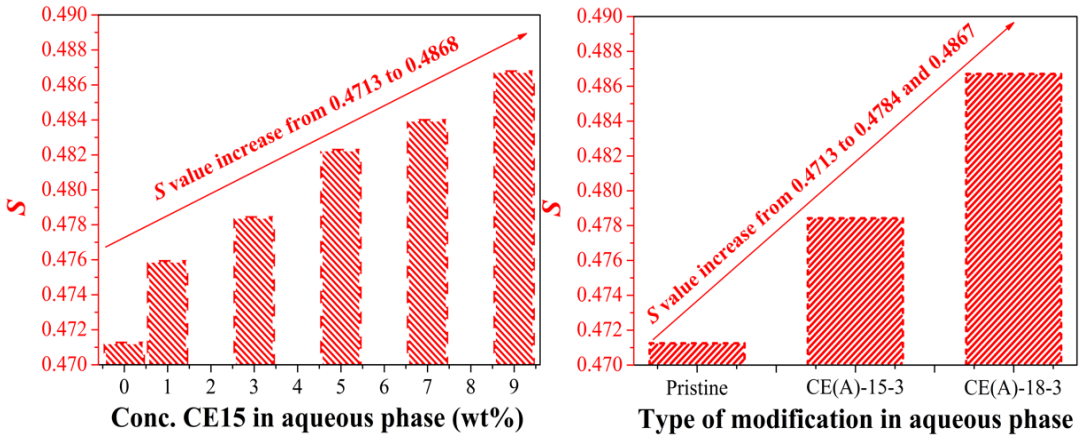

(b)

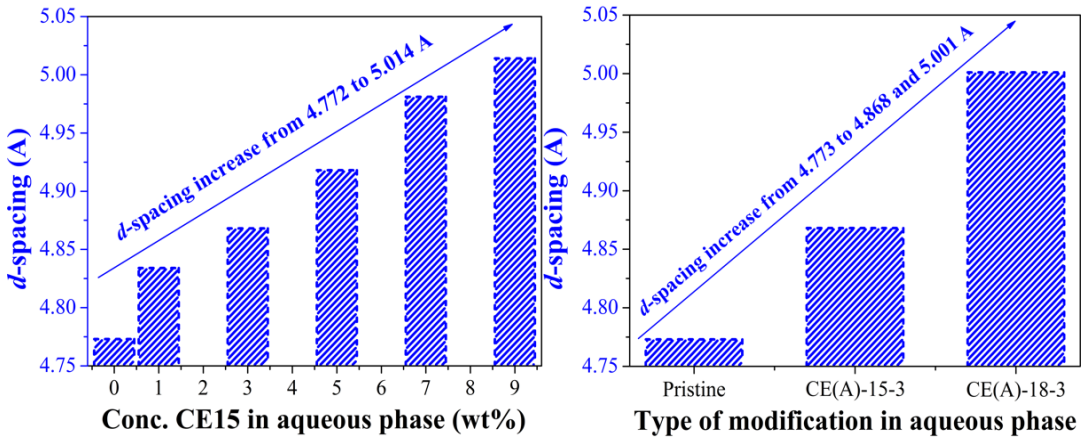

FIGURE 4 (a) *S* and **(b)** *d*-spacing values of the pristine and CE-modified membranes

3.2 Separation performance, antifouling property, and long-term stability

Compared to pristine PA membranes, the larger free volume, higher surface hydrophilicity and rougher surface (larger transport area for water molecules)[48] of the PA layers containing 1 – 7 wt.% CE15 enhanced water flux by 164% during FO operation were (**Figure 5**). However, as CE15 content increased to 9 wt.%, the thickness of the selective layer increased to 389.47±28.69 nm that consequently reduced the water flux by 14% and 17% in FO and PRO modes respectively. Different from typical membrane modifications that increase reverse salt fluxes, the addition of CE15 reduced reverse salt fluxes as a function of higher CE content during modification. This was due to the combination of thicker PA layers, the chelation of CE15 with sodium ions and the repulsion effect of trapped NaCl molecules.

Alternatively, we added both CEs into the organic phase during IP. This approach was impractical as unstable membranes that discolored after IP were formed (**Figure S8**). Membrane discoloration observed here could be due to the dehydration of

amine-saturated substrates caused by CE attraction. Additionally, PA layers modified with CE in the organic phase became yellow and shrank after freeze drying, and delaminated from the discolored PSf substrate (**Figure S8**). PA delamination resulted from the inability to achieve polymer intrusion into the pores during IP, leading to less anchoring sites. The combination of delamination and poor chemical resistance in PA membranes modified with organic phase CE led to significantly higher water fluxes when compared to those of pristine membranes (**Figure 5b**). However, the reverse salt fluxes of these CE(O) membranes were also 11-15 times higher than that of pristine membranes.

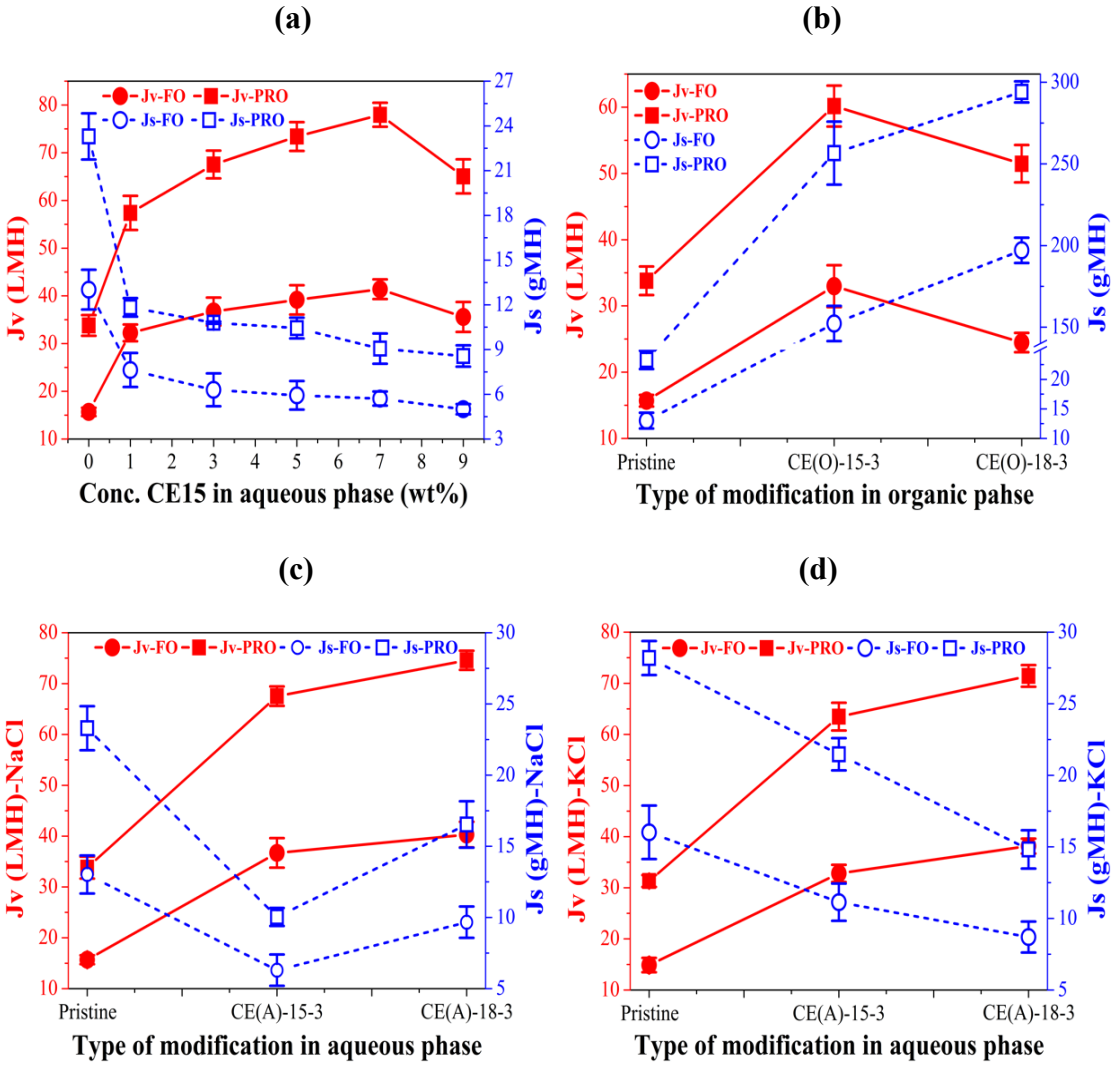

FIGURE 5 FO performance of the pristine membrane and modified membranes **(a)**

with different CE15 loadings added in the aqueous phase; **(b)** with different CEs added in the organic phase; with different CEs added in the aqueous phase using **(c)** NaCl or **(d)** KCl as the draw solution

To investigate the chelation ability of the CE15 and CE18 with Na^+ and K^+ ions, respectively, we employed draw solutions that contained 2M NaCl or KCl draw solution during FO separation (**Figures 5c-d).** The water fluxes of CE-modified TFC membranes in both FO and PRO modes increased as a function of CE cavity size i.e. water fluxes of CE-18 modified membranes were higher than that of CE-15 modified membranes. The osmotic pressure of these two draw solutions were nearly equal,[49] hence resulting in 4-7% change in water flux, regardless membrane modification. However, the reverse salt fluxes of these TFC membranes with the two different draw solutions were vastly different. With NaCl draw solutions, the reverse salt flux of pristine PA membranes was 23% and 21% lower than that with KCl draw solution under FO and PRO mode. This was due to the smaller hydration radius of KCl. The reverse salt flux of PA membranes modified with CE15 was reduced by 57%, from 23.29 gMH to 10.03 gMH when NaCl draw solutions were employed. The reduction in reverse salt flux was only 24% CE15-modified PA membranes when KCl draw solutions were employed. The lower reverse NaCl flux of CE15-modified membranes was attributed to the stronger chelation ability between CE15 and Na^+ ions, and smaller hydration radius of KCl. However, this was not the case for CE18-modified PA membranes where the reverse salt flux was lower when KCl draw solutions were deployed during FO and PRO. This was in spite of the smaller hydration radius of

KCl when compared to NaCl molecules. Clearly, the chelation ability CE18 with K^+ ions played a more dominant role here. Compare to CE15-modified membranes, the reverse salt flux of CE18 membranes towards KCl draw solution was 31% lower, even when the cavity size of CE18 molecules were larger. EDX characterization were performed to quantify metal ion content in the membranes after FO tests (**Table 1** and **Figure S9)**. After FO test with NaCl draw solution, the Na content trapped in CE15-modified membranes was 2.27%, 6 times higher than that in CE18-modified PA membranes. Meanwhile, after FO test with KCl draw solution, K content in CE18-modified membranes were 139% higher than that in CE15-modified membranes, confirming the stronger chelation ability of CE18 with K^+ ions.

TABLE 1 Elemental composition of the pristine and CE-modified membranes after FO tests using different draw solutes

Membrane code	C	N	O	Cl	Na	K
Pristine-NaCl	58.34	11.86	28.38	0.87	0.55	0.00
Pristine-KCl	58.61	10.18	30.16	0.63	0.00	0.42
CE(A)-15-3-NaCl	58.73	9.27	28.14	1.58	2.27	0.00
CE(A)-15-3-KCl	59.22	8.95	31.28	0.05	0.00	0.51
CE(A)-18-3-NaCl	58.75	9.50	31.36	0.09	0.30	0.00
CE(A)-18-3-KCl	58.35	6.53	32.74	1.17	0.00	1.22

The fouling resistance of polymer membranes is crucial for determining the quality of processed water and membrane lifespan.[50] Anti-fouling properties of

membranes studied here were investigated using synthetic wastewater containing SA and calcium ions in the feed solution. Calcium ions acted as the bridge to crosslink SA molecules, forming a SA gel layer on membrane surfaces.[51] The formed SA gel layer could enhance both transport resistance that reduces water permeation,[51] and osmotic pressure to significantly reduce the effective transmembrane osmotic pressure difference.

Upon fouling, the water flux of pristine PA membranes was reduced by 60%, reaching 6.5 LMH as shown in **Figures 6a** and **S10**. There as a 40% loss in water flux even after physical cleaning as the water recovery ratio only reached 60%. Meanwhile, the impact of fouling on the water flux of CE-modified membranes was less prominent where water fluxes were reduced by 24% and 30% for CE15- and CE18-modified membranes respectively. However, we were able to recover 95% of the water flux after physical washes. The improved anti-fouling properties of CE-modified membranes were ascribed to surface hydrophilicity and less reactive carboxylic acid groups. The predominant factor was surface hydrohpilicity where the oxygen atoms in CE behaved as hydrogen bond acceptors,[51] attracting water molecules onto the membrane surface to form a hydration layer that prevented the adsorption of SA molecules. Additionally, the more complete IP reaction in CE-modified membranes contained less carboxylic acid groups on the PA layer that typically function as complexation sites to chelate calcium ions.[51,52]

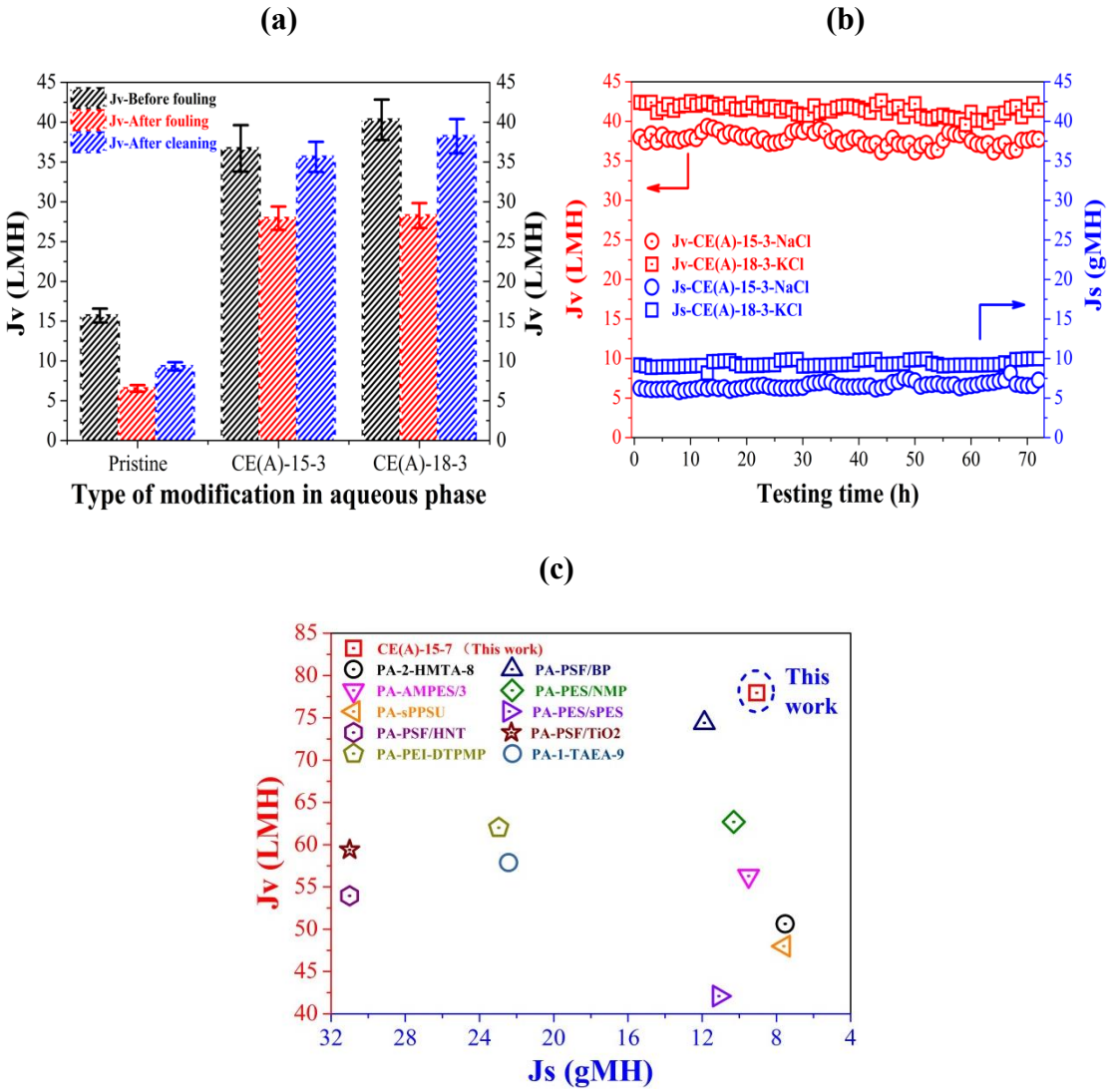

FIGURE 6 (a) Dynamic fouling test results of the pristine and CE-modified membranes; **(b)** long-term FO test results of CE-modified membranes; **(c)** FO performance comparison with recently reported TFC membranes with various modifications (DI water and 2 M NaCl used as the feed and draw solutions, PRO mode)

We also investigated the stability of embedded CE within the modified PA layers via long-term FO tests and vigorous shaking treatments. CE-modified membranes exhibited stable water fluxes over continuous 72 h FO tests (**Figures 6b** and **S11**). Additionally, the reverse salt fluxes of CE-modified membranes increased by only

9-12%, which was possibly due to the concentration effect of the feed solution. The above results demonstrated that the FO performance of CE-modified TFC membranes could be maintained in long term operation, inferring the stability of CE modifiers in modified PA layers during FO operation. PAS and XRD characterization of membranes after long term FO operation revealed that the *S* parameter value decreased by 0.10-0.11% and the *d*-space decreased by 0.25-0.28% Å (**Table 2 and Figure S12)**. These slightly smaller values suggested that the decrease in the free volume content of modified membranes was mainly underpinned by a reduction in intrinsic cavity free volume of CEs. It also could indirectly reflect that the increment in the free volume of CE-modified PA layer was mainly contributed by the larger aggregate and network pores (i.e. the enlarged spatial distance)[22]. We also deployed a TOC analyzer to characterize the amount of CE released from the membranes after vigorous shaking (**Figure S13).** The average CE release rates of CE15-membranes and CE18-membranes during the 7-day shaking treatment are 0.064±0.02 and 0.055±0.01 ppm/cm^2·day, respectively, which further confirmed the stable CE-driven modification of the PA selective layer. The stability of CE modifications, creation of additional porosity whilst facilitating complete IP reactions underpinned the superior separation performances of PA membranes containing 7 wt.% of CE15 molecules. The FO performance of this membrane was more superior than those of various state-of-the-art TFC-PA membranes as displayed in **Figure 6c**,[23,33,53-60] highlighting the feasibility of our approach.

TABLE 2 *S* and 2 theta values of CE-modified membranes before and after long term FO tests

Membrane code	*S*	*d*-spacing (Å)
CE(A)-15-3	0.4784	4.868
CE(A)-15-3-NaCl	0.4779	4.856
CE(A)-18-3	0.4867	5.001
CE(A)-18-3-KCl	0.4864	4.987

4. CONCLUSIONS

In the present study, we investigated the use of two identical CEs, CE15 and CE18, as additives in the aqueous monomer phase to modify the PA selective layer of resultant TFC membranes. Miscibility with hexane and the ability to hydrogen bond with MPD molecules render CE as an efficient phase-transfer catalyst and co-solvent that facilitated the diffusion of MPD molecules into the organic phase during IP. Consequently, PA layers with higher crosslinking degrees and rougher surfaces were achieved. Additionally, the incorporation of CE into the PA layer imbued higher membrane surface hydrophilicity and higher free volume content. This was ascribed to the polar ether groups and intrinsic cavities in CE as well as the enlarged spatial distance of PA chains. Moreover, in comparison with pristine PA membranes, the water fluxes of CE-modified membranes were enhanced by 164% and increased with higher CE concentration or larger CE variants. Crucially, the use of CE during IP lowered reverse salt fluxes of CE-modified membranes. We also demonstrated that chelation abilities with Na^+ or K^+ ions could be harnessed to tailor higher solute rejections of CE15- and CE18-modified membranes with suitable draw solutions. CE-modified membranes were less prone to fouling because of their higher surface

hydrophilicity and lower carboxylic content in the PA layer. The stable embedment of CE into the modified PA layer was also testified by long-term FO test. More importantly, our approaches of CE modification and CE-assisted IP produced FO membranes with state-of-the-art separation performances in a facile manner. This modification approaches could be extended to produce polymer membranes for nanofiltration and gas separations, potentially impacting other important separation applications.

ACKNOWLEDGMENTS

We thank the financial support from National Key Technology Support Program (no. 2014BAD12B06), National Natural Science Foundation of China (no. 21306058), and Natural Science Foundation of Hubei Scientific Committee (no. 2016CFA001). We also appreciate Prof. Tai-Shung Chung in National University of Singapore for PAS characterization. Special thanks are also given to the Analysis and Testing Center, the Analysis and Testing Center of Chemistry and Chemical Engineering School, and the State Key Laboratory of Materials Processing and Die & Mould Technology, in Huazhong University of Science and Technology for their help with material characterizations.

REFERENCES

1. Jones S, Anderson M. Global population set to hit 9.7 billion people by 2050 despite fall in fertility. *The Guardian.* 2015.

2. Elimelech M, Phillip WA. The future of seawater desalination: energy, technology, and the environment. *Science.* 2011;333(6043):712-717.

3. Cheng XQ, Wang ZX, Zhang Y, Zhang Y, Ma J, Shao L. Bio-inspired loose

nanofiltration membranes with optimized separation performance for antibiotics removals. *Journal of membrane science.* 2018;554:385-394.

4. Lieu Le N, Quilitzsch M, Cheng H, et al. Hollow fiber membrane lumen modified by polyzwitterionic grafting. *Journal of Membrane Science.* 2017/01/15/ 2017;522:1-11.

5. Huang Y, Feng X. Polymer-enhanced ultrafiltration: Fundamentals, applications and recent developments. *Journal of Membrane Science.* 2019.

6. Shen L, Zhang X, Zuo J, Wang Y. Performance enhancement of TFC FO membranes with polyethyleneimine modification and post-treatment. *Journal of Membrane Science.* 2017;534:46-58.

7. Le NL, Nunes SP. Ethylene glycol as bore fluid for hollow fiber membrane preparation. *Journal of Membrane Science.* 2017/07/01/ 2017;533:171-178.

8. Le NL, Ulbricht M, Nunes SP. How do polyethylene glycol and poly (sulfobetaine) hydrogel layers on ultrafiltration membranes minimize fouling and stay stable in cleaning chemicals? *Industrial & Engineering Chemistry Research.* 2017;56(23):6785-6795.

9. Huang Y, Sun J, Wu D, Feng X. Layer-by-layer self-assembled chitosan/PAA nanofiltration membranes. *Separation and Purification Technology.* 2018;207:142-150.

10. Yao Z, Yang Z, Guo H, Ma X, Dong Y, Tang CY. Highly permeable and highly selective ultrathin film composite polyamide membranes reinforced by reactable polymer chains. *Journal of colloid and interface science.* 2019/09/15/ 2019;552:418-425.

11. Yi M, Lau CH, Xiong S, et al. Zwitterion-Ag Complexes That Simultaneously Enhance Biofouling Resistance and Silver Binding Capability of Thin Film

Composite Membranes. *ACS applied materials & interfaces.* May 1 2019;11(17):15698-15708.

12. Yang Z, Guo H, Yao Z-k, Mei Y, Tang CY. Hydrophilic Silver Nanoparticles Induce Selective Nanochannels in Thin Film Nanocomposite Polyamide Membranes. *Environmental science & technology.* 2019;53(9):5301-5308.

13. Gai W, Zhao DL, Chung T-S. Thin film nanocomposite hollow fiber membranes comprising Na+-functionalized carbon quantum dots for brackish water desalination. *Water research.* 2019;154:54-61.

14. Shen L, Xiong S, Wang Y. Graphene oxide incorporated thin-film composite membranes for forward osmosis applications. *Chemical Engineering Science.* 2016;143:194-205.

15. Zhang X, Xiong S, Liu C-X, et al. Confining migration of amine monomer during interfacial polymerization for constructing thin-film composite forward osmosis membrane with low fouling propensity. *Chemical Engineering Science.* 2019;207:54-68.

16. Shen L, Zhang X, Tian L, et al. Constructing substrate of low structural parameter by salt induction for high-performance TFC-FO membranes. *Journal of Membrane Science.* 2020;600:117866.

17. Hoehn HH, Richter JW. Aromatic polyimide, polyester and polyamide separation membranes: Google Patents; 1975.

18. Lau WJ, Ismail AF, Misdan N, Kassim MA. A recent progress in thin film composite membrane: A review. *Desalination.* 2012;287:190-199.

19. Shen L, Wang Y. Efficient surface modification of thin-film composite membranes with self-catalyzed tris(2-aminoethyl)amine for forward osmosis separation. *Chemical Engineering Science.* 2018;178:82-92.

552 **20.** Cao X-L, Guo J-L, Cai J, et al. The encouraging improvement of polyamide
553 nanofiltration membrane by cucurbituril-based host-guest chemistry. *AIChE*
554 *Journal*.n/a(n/a).
555 **21.** Lu T-D, Chen B-Z, Wang J, et al. Electrospun nanofiber substrates that
556 enhance polar solvent separation from organic compounds in thin-film
557 composites. *Journal of Materials Chemistry A.* 2018;6(31):15047-15056.
558 **22.** Kim SH, Kwak S-Y, Suzuki T. Positron annihilation spectroscopic evidence to
559 demonstrate the flux-enhancement mechanism in morphology-controlled
560 thin-film-composite (TFC) membrane. *Environmental science & technology.*
561 2005;39(6):1764-1770.
562 **23.** Shen L, Zuo J, Wang Y. Tris(2-aminoethyl)amine in-situ modified thin-film
563 composite membranes for forward osmosis applications. *Journal of Membrane*
564 *Science.* 2017;537:186-201.
565 **24.** Ma X-H, Yao Z-K, Yang Z, et al. Nanofoaming of Polyamide Desalination
566 Membranes To Tune Permeability and Selectivity. *Environmental Science &*
567 *Technology Letters.* 2018;5(2):123-130.
568 **25.** Shen L, Hung W-s, Zuo J, Zhang X, Lai J-Y, Wang Y. High-performance
569 thin-film composite polyamide membranes developed with green
570 ultrasound-assisted interfacial polymerization. *Journal of Membrane Science.*
571 2019;570-571:112-119.
572 **26.** Shen L, Hung W-s, Zuo J, et al. Effect of ultrasonication parameters on
573 forward osmosis performance of thin film composite polyamide membranes
574 prepared with ultrasound-assisted interfacial polymerization. *Journal of*
575 *Membrane Science.* 2020;599:117834.
576 **27.** Gu JE, Lee S, Stafford CM, et al. Molecular layer-by-layer assembled

577 thin-film composite membranes for water desalination. *Advanced materials.*
578 Sep 14 2013;25(34):4778-4782.
579 **28.** Karan S, Jiang Z, Livingston AG. Sub–10 nm polyamide nanofilms with
580 ultrafast solvent transport for molecular separation. *Science.*
581 2015;348(6241):1347-1351.
582 **29.** Chowdhury MR, Steffes J, Huey BD, McCutcheon JR. 3D printed polyamide
583 membranes for desalination. *Science.* 2018;361(6403):682-686.
584 **30.** Wang Z, Wang Z, Lin S, et al. Nanoparticle-templated nanofiltration
585 membranes for ultrahigh performance desalination. *Nature communications.*
586 2018;9(1):2004.
587 **31.** Yoshio M, Noguchi H. Crown ethers for chemical analysis: A Review.
588 *Analytical Letters.* 1982;15(15):1197-1276.
589 **32.** Steed JW. First-and second-sphere coordination chemistry of alkali metal
590 crown ether complexes. *Coordination Chemistry Reviews.*
591 2001;215(1):171-221.
592 **33.** Shen L, Tian L, Zuo J, Zhang X, Sun S, Wang Y. Developing
593 high-performance thin-film composite forward osmosis membranes by various
594 tertiary amine catalysts for desalination. *Advanced Composites and Hybrid*
595 *Materials.* March 01 2019;2(1):51-69.
596 **34.** Shen L, Yi M, Tian L, et al. Efficient surface ionization and metallization of
597 TFC membranes with superior separation performance, antifouling and
598 anti-bacterial properties. *Journal of Membrane Science.* 2019;586:84-97.
599 **35.** Oehrle SA. Controlled changes in selectivity of cation separations by capillary
600 electrophoresis using various crown-ether additives. *Journal of*
601 *Chromatography A.* 1996;745(1-2):87-92.

602 **36.** Maleknia S, Brodbelt J. Cavity-size-dependent dissociation of crown
603 ether/ammonium ion complexes in the gas phase. *J.am.chem.soc.*
604 1993;115(7):2837-2843.
605 **37.** Ouchi M, Inoue Y, Kanzaki T, Hakushi T. Molecular design of crown ethers. 1.
606 Effects of methylene chain length: 15-to 17-crown-5 and 18-to 22-crown-6.
607 *The Journal of Organic Chemistry.* 1984;49(8):1408-1412.
608 **38.** Zhang H, Chu IH, Leming S, Dearden DV. Gas-phase molecular recognition:
609 gas-phase crown ether-alkali metal ion complexes and their reactions with
610 neutral crowns. *Journal of the American Chemical Society.*
611 1991;113(19):7415-7417.
612 **39.** Ong RC, Chung T-S. Fabrication and positron annihilation spectroscopy (PAS)
613 characterization of cellulose triacetate membranes for forward osmosis.
614 *Journal of membrane science.* 2012;394:230-240.
615 **40.** Belfer S, Purinson Y, Kedem O. Surface modification of commercial
616 polyamide reverse osmosis membranes by radical grafting: An ATR-FTIR
617 study. *Acta Polymerica.* 1998;49(10-11):574-582.
618 **41.** Gherrou A, Kerdjoudj H, Molinari R, Seta P, Drioli E. Fixed sites plasticized
619 cellulose triacetate membranes containing crown ethers for silver(I), copper(II)
620 and gold(III) ions transport. *Journal of Membrane Science.* 2004/01/15/
621 2004;228(2):149-157.
622 **42.** Li Y, Zhao JQ, Yuan YC, et al. Polyimide/Crown Ether Composite Films with
623 Necklace-Like Supramolecular Structure and Improved Mechanical, Dielectric,
624 and Hydrophobic Properties. *Macromolecules.* 2015/04/14
625 2015;48(7):2173-2183.
626 **43.** Kwon Y-N, Hong S, Choi H, Tak T. Surface modification of a polyamide

reverse osmosis membrane for chlorine resistance improvement. *Journal of Membrane Science.* 2012/10/01/ 2012;415-416:192-198.

44. Chae H-R, Lee J, Lee C-H, Kim I-C, Park P-K. Graphene oxide-embedded thin-film composite reverse osmosis membrane with high flux, anti-biofouling, and chlorine resistance. *Journal of Membrane Science.* 2015;483:128-135.

45. Chen H, Hung W-S, Lo C-H, et al. Free-volume depth profile of polymeric membranes studied by positron annihilation spectroscopy: layer structure from interfacial polymerization. *Macromolecules.* 2007;40(21):7542-7557.

46. An Q, Hung W-S, Lo S-C, et al. Comparison between Free Volume Characteristics of Composite Membranes Fabricated through Static and Dynamic Interfacial Polymerization Processes. *Macromolecules.* 2012;45(8):3428-3435.

47. Kong X, Qiu Z-L, Lin C-E, et al. High permselectivity hyperbranched polyester/polyamide ultrathin films with nanoscale heterogeneity. *Journal of Materials Chemistry A.* 2017;5(17):7876-7884.

48. Tan Z, Chen S, Peng X, Zhang L, Gao C. Polyamide membranes with nanoscale Turing structures for water purification. *Science.* 2018;360(6388):518-521.

49. Cath TY, Childress AE, Elimelech M. Forward osmosis: Principles, applications, and recent developments. *Journal of Membrane Science.* 2006/09/15/ 2006;281(1):70-87.

50. Zhang R, Liu Y, He M, et al. Antifouling membranes for sustainable water purification: strategies and mechanisms. *Chem Soc Rev.* Oct 24 2016;45(21):5888-5924.

51. Lu X, Romero-Vargas Castrillon S, Shaffer DL, Ma J, Elimelech M. In situ

652 surface chemical modification of thin-film composite forward osmosis
653 membranes for enhanced organic fouling resistance. *Environmental science &*
654 *technology.* 2013;47(21):12219-12228.
655 **52.** Xie M, Gray SR. Gypsum scaling in forward osmosis: Role of membrane
656 surface chemistry. *Journal of Membrane Science.* 2016;513:250-259.
657 **53.** Zhang X, Tian J, Ren Z, et al. High performance thin-film composite (TFC)
658 forward osmosis (FO) membrane fabricated on novel hydrophilic disulfonated
659 poly(arylene ether sulfone) multiblock copolymer/polysulfone substrate.
660 *Journal of Membrane Science.* 2016;520:529-539.
661 **54.** Qiu M, Wang J, He C. A stable and hydrophilic substrate for thin-film
662 composite forward osmosis membrane revealed by in-situ cross-linked
663 polymerization. *Desalination.* 2018;433:1-9.
664 **55.** Sukitpaneenit P, Chung TS. High performance thin-film composite forward
665 osmosis hollow fiber membranes with macrovoid-free and highly porous
666 structure for sustainable water production. *Environmental science &*
667 *technology.* Jul 3 2012;46(13):7358-7365.
668 **56.** Widjojo N, Chung T-S, Weber M, Maletzko C, Warzelhan V. A sulfonated
669 polyphenylenesulfone (sPPSU) as the supporting substrate in thin film
670 composite (TFC) membranes with enhanced performance for forward osmosis
671 (FO). *Chemical Engineering Journal.* 2013;220:15-23.
672 **57.** Sahebi S, Phuntsho S, Woo YC, et al. Effect of sulphonated polyethersulfone
673 substrate for thin film composite forward osmosis membrane. *Desalination.*
674 2016;389:129-136.
675 **58.** Ghanbari M, Emadzadeh D, Lau WJ, Riazi H, Almasi D, Ismail AF.
676 Minimizing structural parameter of thin film composite forward osmosis

membranes using polysulfone/halloysite nanotubes as membrane substrates. *Desalination.* 2016/01/01/ 2016;377:152-162.

59. Emadzadeh D, Lau WJ, Matsuura T, Ismail AF, Rahbari-Sisakht M. Synthesis and characterization of thin film nanocomposite forward osmosis membrane with hydrophilic nanocomposite support to reduce internal concentration polarization. *Journal of Membrane Science.* 2014;449:74-85.

60. Shen L, Wang F, Tian L, Zhang X, Ding C, Wang Y. High-performance thin-film composite membranes with surface functionalization by organic phosphonic acids. *Journal of Membrane Science.* 2018;563:284-297.